RSC Advances

ROYAL SOCIETY OF CHEMISTRY

www.rsc.org/advances

RSC Advances

COMMUNICATION

Real time imaging of the growth of silver ribbons by evanescent wave microscopy

Received 00th January 20xx,

Accepted 00th January 20xx

DOI: 10.1039/x0xx00000x

www.rsc.org/

Angshuman Pal,[a] Panart Khajornrungruang,[b] and S. V. Babu*[a]

Real time visualization of the *in situ* growth of ~40 µm long high aspect ratio silver ribbons, synthesized by template-free galvanic displacement using ~100nm Cu particles and Ag ions in aqueous conditions, is demonstrated using evanescent wave microscopy. The observed growth rate from several ribbons is 1.5 ± 0.5 µm/s.

In situ measurement and real time imaging of nanostructures have attracted a great deal of interest since they can shed light on their growth dynamics. In situ liquid transmission electron microscopy (TEM) was used to observe the growth of lead sulphide nanoparticles [1] and growth of single colloidal platinum nanocrystals [2], both in real time. Liao et al. were able to image in real time by TEM the growth of Pt_3Fe nanoparticles and nanorods in solution, initiated by e-beam exposure.[3] However, while the use of TEM enabled the characterization of the growth process of these materials, these types of measurements need complex sample preparation methods and a sealed environment with high vacuum. Also, samples with low volatile solvents or biological cells in aqueous media or with intrinsic cellular water cannot with stand exposure to an electron beam and, hence, cannot be imaged using these TEM based methods. A recent review [4] describes electron microscopy imaging methods using Au nanoparticle labelling that can overcome some of these limitations, but all these methods also require very sophisticated and costly instrumentation.

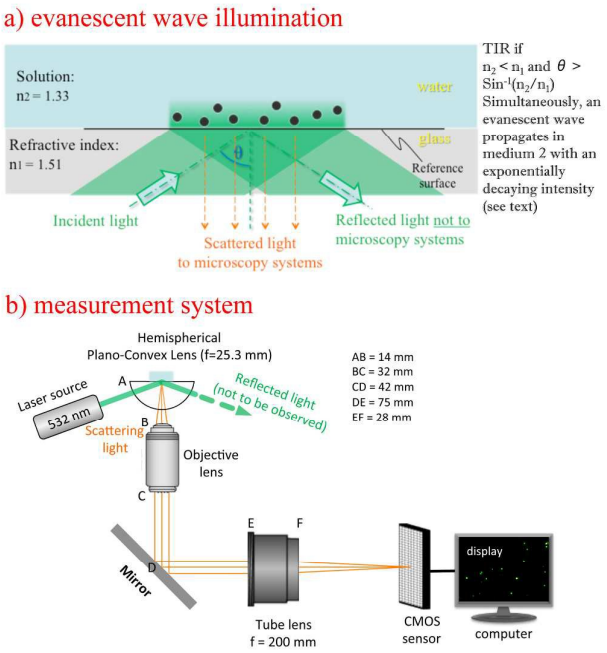

Fig. 1: (a) Evanescent wave illumination and (b) ray diagram of EW microscopy. The EW penetration depth is typically ~100 – 200 nm.

In contrast, evanescent wave (EW) light-scattering technique or microscopy [5-9] does not suffer from these limitations. This EW scattering imaging method, initially introduced by Prieve et al. [10], relies on total internal reflection (TIR) and was used to study both equilibrium and dynamic behavior of charged particles near a flat surface.[11] At present, however, no commercial compact equipment is available for EW microscopy. Here we demonstrate a simple and easy-to-build EW microscopy system by modifying a recently proposed experimental system [9] and demonstrate its use to

[a] *Center of Advance Materials Processing, Clarkson University Potsdam, NY, 13676 USA *Corresponding Author: Email: babu@clarkson.edu*
[b] *Dept. of Mechanical Information Science and Technology, Kyushu Institute of Technology, Iizuka-shi, Fukuoka, Japan*
Electronic Supplementary Information (ESI) available: [details of any supplementary information available should be included here]. See DOI: 10.1039/x0xx00000x

observe in real time the *in situ* growth of high aspect ratio (~40 μm length and ~ 60 to 100 nm wide) silver nano-ribbons. It is a powerful technique that can be used to capture both images and video with nanoscale resolution and for dynamic observations of the formation and growth of nanostructures.

EW microscopy uses the EW produced by the TIR of a light beam from a glass/liquid interface to illuminate a layer of any material present in the liquid below the glass and lies within the penetration depth (~ 100 to 200 nm) [5,12] of the evanescent field as shown in figure 1a. When light travels from a medium with a high refractive index (RI) n_1 into a low RI medium (sample fluid) with RI n_2, TIR occurs if the incident angle is larger than the critical angle $\theta_c = \sin^{-1}(n_2/n_1)$. When TIR occurs, a small fraction of the light energy penetrates into the low RI medium and propagates (the EW) parallel to the surface, with an intensity that decays exponentially in the direction perpendicular to the propagation direction. [8,10] The penetration depth, which characterizes the evanescent field, can be calculated as: $d = \lambda_0/4\pi(n_1^2\sin^2\theta - n_2^2)^{-1/2}$; where d is the evanescent wave penetration depth, λ_0 is the wavelength of the incident light and θ is the incident angle.[5] When a particle (black spheres in figure 1a) is located in the EW field, it will scatter the wave with an intensity that depends on its distance from the interface and its size. A ray diagram of our experimental evanescent light scattering system is shown in figure 1b. A laser diode (532 nm and 15 mW) was used as the light source. The scattered signal from the propagating light is collected by an area sensor of a CMOS digital camera with an objective lens (CF IC EPI Plan SLWD Ultra-long working distance objective from Nikon, Japan; magnification = 50x, NA = 0.45, working distance = 13.8 mm) and an infinity-corrected tube lens (ITL 200, THORLABS, USA; focal length = 200 mm). The tube lens can be used to adjust the distance between the detector and the reflecting mirror (figure 1b). Liquid drops containing the reactants were placed on a hydrophobic (contact angle: 76°) antireflective (AR) film coated plano-convex lens (LA1951-A, THORLABS, USA; focal length = 25.3 mm; coating thickness = 350-700 nm) and imaged. The hydrophobic nature of the planar lens surface helps in retaining a spherical shape for the liquid sample. This home-built EW imaging system was used to image Cu particles (~100 nm dia.) and capture videos (100 frames/s) in real time of the growing high aspect ratio Ag nano-ribbons.

The silver nano-ribbons were grown in solution by galvanic displacement, based on the well-known redox reaction between metallic copper and Ag ions [13-16] without using any additives or templates. This is a straightforward aqueous route for the production of silver ribbons with good crystalline quality. This protocol does not rely on any dispersants/capping agents commonly used to improve nanoparticle uniformity and/or to tailor particle shape during conventional chemical precipitation methods used for the preparation of many types of metallic particles. [17-20] Since there is no template, we obtain pristine Ag surfaces for the growing ribbons, a highly desirable characteristic for studying their nucleation and growth in real time.

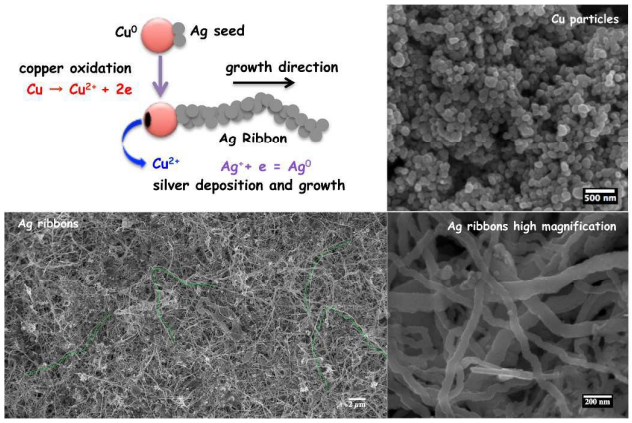

Fig. 2: The growth mechanism and SEM images of the Cu nanoparticles and the silver ribbons that were grown. Some of the ribbons (traced by the green lines) are ~ 60 μm long

In our experiments, Cu nanoparticles (average size 100 nm) were dispersed (0.1 wt %) in deionized water (18Ω) and a drop of (40 μL) this dispersion was placed onto the flat surface of the glass lens (figure 1b) followed by the addition of a 60 μL of aqueous 0.1M $AgNO_3$ solution. Ag ribbons start forming after a short induction time of about 7±1 s as seen in several experiments and then grow in length with time. A sample of the Ag ribbons/wires grown [after 90 s] was imaged by conventional SEM imaging and shown in figure 2. The few green lines drawn to trace the ribbons in the images show that some of the ribbons are as long as ~ 60 μm.

As these Ag ribbons form and grow, they were imaged *in situ* using the EW imaging system shown in figure 1. The images were acquired with a CMOS camera (Baumer HXC20, pixel size 5.5 μm^2) controlled by Silicon Software (GmbH micro Display 5.2.2). A scale bar was introduced into these images by comparing the pixel size resolution of an already known line-space pattern as well as that of the known pore size of a standard TEM grid (details in the supporting information S-1) similar to what was already reported earlier. [9] The resolution was found to be 13.37 pixels = 1μm.

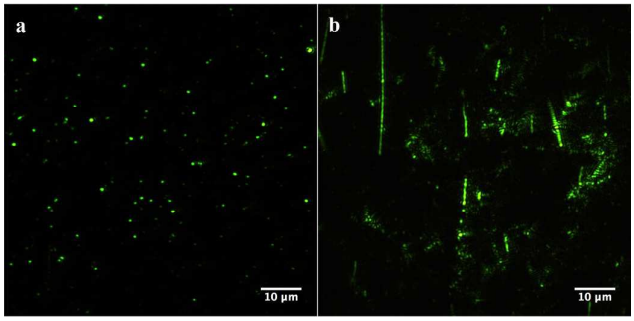

Fig. 3: Evanescent wave scattering images of (a) starting ~ 100 nm Cu particles and (b) silver ribbons after 90s of growth.

Figure 3a and 3b show the evanescent wave scattering images of the starting Cu particles and the growing Ag ribbons observed after 90 s, respectively. In figure 3b, several Ag ribbons with a wide distribution of lengths can be seen, with one of them reaching a length of over 40 µm. Even though the number of ribbons formed in the small sample liquid drop is quite large (See the SEM image, figure 2), only the small fraction of them that is present in the evanescent field and is growing more or less parallel to the glass-water interface is observed by EW imaging. The intensity of the evanescent images varies based on exposure time and, at fixed exposure time, on their distance from the glass-water interface, with closer objects having higher intensity. Since the intensity also increases with the size of the objects, [9] an exposure time of 20 ms was used to image the smaller 100 nm Cu particles while an exposure time of 2 ms was adequate to image the bigger micron scale silver ribbons. Images of the growing silver ribbons obtained at six different growth times (up to 70 s) from one particular observation spot on the glass surface are shown in figure 4. Quite a few growing ribbons (four intense ribbons are labelled as *a*, *b*, *c* and *d*) of variable length can be identified with brightness that is related to both their size and distance from the interface. All of them seem to start from different Cu particles – one for particle. Ribbon *b*, one of the more intense ones, appears after ~ 20 s and grows to ~ 30 µm, first rapidly and then more slowly [We determine the growth rate of the ribbons more precisely from the video images below]. Some remain faint, more likely indicative of their location near the waning portion of the EW. Several point images that do not grow in size can also be seen and most of them remain fixed in size and/or intensity. They are most likely the Cu particles that diffused to the glass surface and adhered to it. Also, no dendrites were observed unlike in the experiments reported by Liu and Sen and Avizienis et al, [13,14] perhaps due to the combination of Ag^+ concentration and of the 100 nm size Cu particles used here.

EW microscopy also allows us to image continuously the growing ribbons *in situ* and in real time using the same camera and software. One such video captured over four seconds at 100 frames/s is available in the supporting information (S-2). Longer videos can also be obtained but require considerable computer memory. Figure 5 shows five sequential images of the growing ribbons captured every 1 s from a total of 400 frames (4 s). In this video the image shown at 0.01 s was the 1st frame after the video capture was initiated, which itself was ~7 s (the induction time, mentioned earlier) after the drop of silver nitrate solution was placed on the glass plano-convex lens surface.

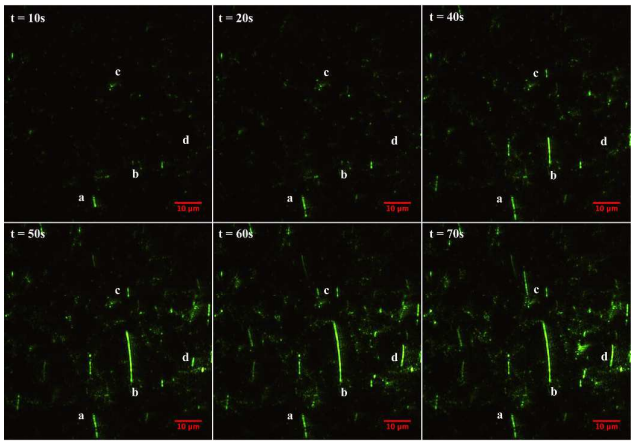

Fig. 4: Formation and growth of ribbons at different times

We now focus attention on the growth dynamics of the three ribbons labelled *a*, *b* & *c*. These ribbons start appearing at different times (frames 2, 115, 58 for *a*, *b*, and *c*, respectively, see the supplemental information video), suggesting different nucleation times, presumably determined by the surface energetics of the Cu particles. The lengths of these three ribbons can be obtained from the images as a function of time using the scale bar shown in figure 5 and are shown in the table 1. There is an initial burst of growth at about ~ 3 µm/s for all the three ribbons but then it drops considerably as the ribbons grow. These ribbons seem to grow in our experiments by the addition of Ag at the growing end of the ribbon. Such a growth process is obviously controlled by Ag^+ availability by diffusion and the potential difference between the end of the growing ribbon and the electron donating Cu particle at the other end of the ribbon.

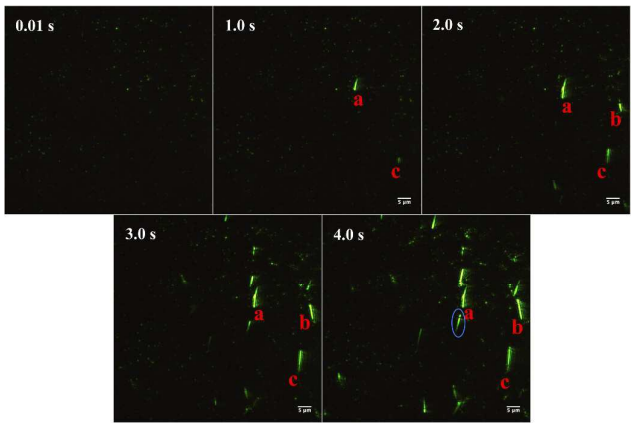

Fig. 5: Sequential images of ribbons obtained from a 4 s video

The images of ribbon *a* in figure 5 at three different times of observation (1.6, 1.8 and 2.0 s) were magnified and shown in figure 6a-c. While most of the growth is occurring at the end, bulging of the ribbon at the middle is also evident. This is quite likely driven by a local fluctuation in the Ag^+ concentration and could be a precursor to incipient dendrite formation. Magnified images of the ribbon circled in figure 5 are shown in figure 6d and e. Figure 6e clearly shows a second ribbon growing, separated by a small distance from its close neighbour. Since the width of the gap between these two ribbons is ~ 250 nm, we can not determine conclusively whether they originated from a large 250 nm Cu cluster or from two distinctly small Cu particles. In any case, it is very interesting that these two ribbons are aligned almost perfectly. Reviewing the images from the earlier figures, it appears that this is not a unique case and there are many such examples.

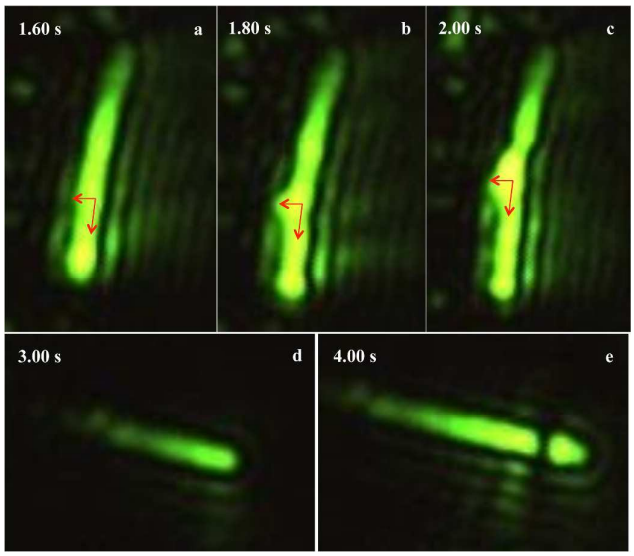

Fig. 6: a, b and c shows magnified images of the ribbon labelled as *a* in figure 5; d and e shows the same for the ribbon enclosed by the circle

The fringes that appear in the above figure are most likely caused by slightly defocused imaging as reported by several authors, for example, [21] or due to Airy disk diffraction pattern.[22]

Based on the analysis of several images and videos (see the supplemental information), the growth rate averaged over several silver ribbons over their entire growth was found to be ~ 1.5 ± 0.5 µm/s, lower than the initial rate of ~ 3.0 µm/s (Table 1). These rates are considerably larger than the 150 - 350 nm/s reported by Liu and Sen [13], who observed a time dependent average growth rate of 345 nm/s in the first 6 s which decreased to 287, 187 and 143 nm/s in three successive 6 s periods.

Time (s)	Length (µm) and Growth rate (µm/s)					
	a	µm/s	b	µm/s	c	µm/s
1	3.1	2.7	-	3.1	1.7	3.2
2	5.8	0.5	2.7	2.6	4.9	2.3
3	6.3	0.2	5.3	2.0	7.2	0.6
4	6. 5		7.3		7.8	

Table 1: length and growth rate of the three ribbons a, b and c identified in figure 5

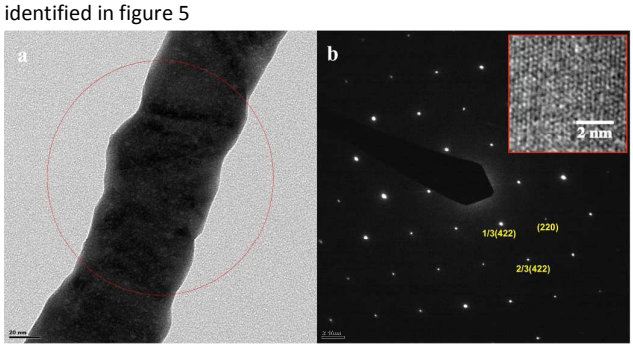

Fig. 7: (a) TEM and (b) ED images of one of the Ag ribbons (inset is a high magnification HRTEM image of the ribbon)

High resolution TEM (HRTEM) and selected area electron diffraction (SAED) images of one of the silver ribbon are shown in figure 7. The crystal plane indexes are marked in the selected area electron diffraction (SAED) pattern in figure 7b. The set with a spacing of 1.44 Å could be indexed to the {220} reflections of fcc silver. The outer set (with a lattice spacing of 0.83 Å) corresponds to the {422} reflections. The other sets are corresponding to the forbidden planes of 1/3{422} and 2/3{422} with d-spacing of 2.5 Å and 1.24 Å, respectively.

Conclusions

We described an evanescent wave scattering imaging method and demonstrated its application to image ~100 nm Cu particles and capture *in situ* real time videos of rapidly growing high aspect ratio 40 μm long Ag ribbons grown by galvanic displacement. This technique is relatively simple and cost-effective, and does not require elaborate sample preparation. The video images captured at 100 frames/s contain a wealth of data and can be used to extract considerable information about the growth dynamics of the Ag nano-ribbons. In our case the ribbon growth rate was ~3 μm/s initially while the average growth rate was 1.5 ± 0.5 μm/s over 40 s. It should be possible to extend this EW approach to the real time imaging of the growth of a multitude of simple and complex nanostructures, including biological systems that are sensitive to electron exposure.

Acknowledgements:

This work was financially supported by the National Science Foundation, USA, through the I/U-CRC Metamaterials Award #1068040. We acknowledge Christopher Plunkett and Armin Vahdat for help with equipment setup, Christopher Netzband for providing Cu particles and Vahid Rastegar for the SAED analysis.

References

1 J. E. Evans, K. L. Jungjohann, N. D. Browning, L. Arslan, *Nano letters* 2011, **11**, 2809
2 H. Zheng, R. K. Smith, Y. W. Jun, C. Kisielowski, U. Dahmen, A. P. Alivisatos, *Science* 2009, **324**, 1309-1312
3 H. G. Liao, L. Cui, S. Whitelam, H. Zheng, *Science* 2012, **336**, 1011
4 N. de Jonge, F. M. Ross, *Nature Nanotechnology* 2011, **6**, 695
5 M. Hosoda, K. Saki, K. Takagi, *Physical Rev. E* 1998, **58**, 6275
6 H. He, J. Ren, *Talanta* 2008, **77**, 166
7 S. Lee, G. Park, S. K. Chakkarapani, S. H. Kang, *Biosensors and Bioelectronics*, 2015, **63**, 444
8 M. Oheim, *Laser Med Sci* 2001, **16**, 159
9 P. Khajornrungruang, P. J. Dean, S. V. Babu, *Proc. of Annual Meeting of the American Society for Precision Engineering* 2014, **29**, 73
10 D. C. Prieve, F. Luo, F. Lanni, Farady Discuss Chem. Soc. 1987, **83**, 297
11 D. C. Prieve, J. Y. Walz, *Applied Optics* 1993, **32**, 1629
12 Y. Kazoe, M. Yoda, *Journal of Fluids Engineering* 2013, **135**, 021305
13 R. Liu, A. Sen, *Chem. Mater.* 2012, **24**, 48
14 A. V. Avizienis, C. M-Olmos, H. O. Sillin, M. Aono, J. K. Gimzewski, A. Z. Stieg *Cryst. Growth Des.* 2013, **13**, 465
15 Z. Wang, Z. Zhao, J. Qiu, *Journal of Physics and Chemistry of solids,* 2008, **69**, 1296
16 X. Sun, L. Lin, Z. Li, Z. Zhang, J. Feng, *Material Lett.* 2009, **63**, 2306
17 D. Goia, E. Maijevic, *New J. Chem.* 1998, **22**, 1203
18 L. Suber, I Sondi, E. Matijevic, D. Goia, *J. Colloid Interface sci.* 2005, **288**, 489
19 A. Pal, I. Sevonkaev, B. Bartling, J. Rijssenbeek, D. V Goia *RSC Adv.* 2014, **4**, 20909
20 A. Pal, S. Shah, S. Devi *Colloids and Surface A: Physicochemical and Engineering Aspects* 2007, **302**, 55
21 T. Motegi, H. Nabika, Y. Niidome, K. Murakoshi *J. Phys. Chem. C* 2013, **117**, 2535
22 Rui Luo and Yan-Fei Sun, Meas. Sci. Technol. 2011, **22**, 045402